Transcriptional regulation of *CYR61* and *CTGF* by LM98: a synthetic YAP-TEAD inhibitor that targets in-vitro vasculogenic mimicry in glioblastoma cells

Marie-Eve Roy[a], Carolane Veilleux[a], Alexis Paquin[b], Alexandre Gagnon[b] and Borhane Annabi[a]

Downloaded from http://journals.lww.com/anti-cancerdrugs by BhDMf5ePHKav1zEoum1tQfN4a+kJLhEZgbsIHo4XMi0hCywCX1AWnYQp/IlQrHD3i3D0OdRyi7TvSFl4Cf3VC4/OAVpDDa8K2+Ya6H515kE= on 07/02/2024

Glioblastoma (GBM) is a highly angiogenic malignancy of the central nervous system that resists standard antiangiogenic therapy, in part because of an alternative process to angiogenesis termed vasculogenic mimicry. Intricately linked to GBM, dysregulation of the Hippo signaling pathway leads to overexpression of YAP/TEAD and several downstream effectors involved in therapy resistance. Little is known about whether vasculogenic mimicry and the Hippo pathway intersect in the GBM chemoresistance phenotype. This study seeks to investigate the expression patterns of Hippo pathway regulators within clinically annotated GBM samples, examining their involvement *in vitro* regarding vasculogenic mimicry. In addition, it aims to assess the potential for pharmacological targeting of this pathway. In-silico analysis of the Hippo signaling members *YAP1*, *TEAD1*, *AXL*, *NF2*, *CTGF*, and *CYR61* transcript levels in low-grade GBM and GBM tumor tissues was done by Gene Expression Profiling Interactive Analysis. Gene expression was analyzed by real-time quantitative PCR from human U87, U118, U138, and U251 brain cancer cell lines and in clinically annotated brain tumor cDNA arrays. Transient gene silencing was performed with specific small interfering RNA. Vasculogenic mimicry was assessed using a Cultrex matrix, and three-dimensional capillary-like structures were analyzed with Wimasis. *CYR61* and *CTGF* transcript levels were elevated in GBM tissues and were further induced when in-vitro vasculogenic mimicry was assessed. Silencing of *CYR61* and *CTGF*, or treatment with a small-molecule TEAD inhibitor LM98 derived from flufenamic acid, inhibited vasculogenic mimicry. Silencing of *SNAI1* and *FOXC2* also altered vasculogenic mimicry and reduced *CYR61/CTGF* levels. Pharmacological targeting of the Hippo pathway inhibits in-vitro vasculogenic mimicry. Unraveling the connections between the Hippo pathway and vasculogenic mimicry may pave the way for innovative therapeutic strategies. *Anti-Cancer Drugs* XXX: XXXX–XXXX Copyright © 2024 The Author(s). Published by Wolters Kluwer Health, Inc.

Anti-Cancer Drugs XXX, **XXX**:XXXX–XXXX

Keywords: chemoresistance, glioblastoma, Hippo pathway, vasculogenic mimicry, YAP/TEAD

[a]Laboratoire d'Oncologie Moléculaire and [b]Laboratoire de Chimie Organique et Médicinale, Département de Chimie, Université du Québec à Montréal, Montreal, Québec, Canada

Correspondence to Borhane Annabi, Laboratoire d'Oncologie Moléculaire, Département de Chimie,Université du Québec à Montréal, C.P. 8888, Succ. Centre-ville, Montréal, QC H3C 3P8, Canada
Tel: +1 514 987 3000 x7610; e-mail: annabi.borhane@uqam.ca

Received 15 May 2024 **Revised form accepted** 16 May 2024.

Introduction

Glioblastomas (GBM) are, according to the Genetic and Rare Diseases (GARD) Information Center from the National Institutes of Health (USA), rare aggressive and malignant grade IV brain tumors that originate from the glial cells of the brain [1]. It is the most common and deadly malignant brain tumor in adults, with a median survival of less than 15 months [2]. Several drugs have been granted an orphan drug designation by the US Food and Drug Administration (FDA) or European Medicines Agency (EMA) for the treatment of GBM, such as azeliragon, bevacizumab, and FLAG-003 [3,4]. Most of them, however, have not been approved for marketing or have shown limited efficacy in clinical trials. Furthermore, overcoming immunotolerance, stimulating robust tumor antigen responses, and countering the immunosuppressive microenvironment is critical for curative GBM immunotherapy [5,6]. Therefore, there still is a high unmet need for new therapeutic strategies for GBM patients, and for a better understanding of the immunosuppressive pathways involved.

Our team has recently developed various molecules that target the Hippo pathway involved in the immunosuppressive nature of GBM tumors [7–9]. This signaling pathway consists of a kinase cascade that inhibits the nuclear translocation of yes-associated protein and its transcriptional coactivator with PDZ-binding motif (YAP/TAZ), which are transcriptional coactivators that promote cell growth and survival [10]. Deregulation of the Hippo pathway in GBM leads to increased YAP/TAZ activity

This is an open-access article distributed under the terms of the Creative Commons Attribution-Non Commercial-No Derivatives License 4.0 (CCBY-NC-ND), where it is permissible to download and share the work provided it is properly cited. The work cannot be changed in any way or used commercially without permission from the journal.

Downloaded from http://journals.lww.com/anti-cancerdrugs by BhDMf5ePHKav1zEoum1tQfN4a+kJLhEZgbsIHo4XMi0hCywCX1AWnYQp/IlQrHD3i3D0OdRyi7TvSFl4Cf3VC4/OAVpDDa8K2+Ya6H515kE= on 07/02/2024

and resistance to chemotherapy and immunotherapy [11]. Given its role in glioma progression and chemoresistance as well as metastasis in several cancers, the Hippo pathway holds promise as a therapeutic target, particularly for high-grade gliomas like GBM [12,13]. The Hippo pathway also interacts with other signaling pathways, such as Wnt, Notch, and epidermal growth factor receptor which are also implicated in GBM development and progression [14]. Concomitantly, our very own previous investigation, which led us to unravel novel pharmacological approaches using new synthetic compounds, may further potentially target Hippo-associated pathways.

The regulation of vasculogenic mimicry, a process in which tumor cells form vascular-like structures to supply blood for tumor growth and metastasis, is associated with poor clinical outcomes and resistance to antiangiogenesis therapies in many cancers, including GBM [15]. The molecular mechanisms underlying vasculogenic mimicry formation are complex and not fully understood, but some studies have suggested that the Hippo pathway may play a key role in this process [16,17]. For example, RNA m6A methylation, a common mRNA modification that regulates gene expression, has been shown to promote vasculogenic mimicry formation in hepatocellular carcinoma via the Hippo pathway [18]. Another study demonstrated that hypoxia, a common feature of the solid tumors microenvironment, induces vasculogenic mimicry formation in GBM cells through the activation of the Hippo pathway [19]. In fact, hypoxia increases the expression and nuclear localization of YAP, which subsequently upregulates the expression of vasculogenic mimicry–related genes, such as *VEGFR1*, *VEGFR2*, and *VE-cadherin*, enhancing the ability of GBM cells to form vasculogenic mimicry networks [20].

Numerous signaling pathways have been studied in gliomas including the Hippo pathway in particular because of the high expression of its effectors YAP/TAZ which correlate with the grade of malignancy, reaching maximal levels in GBM [21]. Patients with TAZ overexpressing tumors exhibit a poor prognosis and, in cell models, TAZ promotes tumor progression, while its knockdown prevents proliferation, tumorigenicity, and invasion of glioma cells [22]. The deregulation of the Hippo pathway represents a mechanism that further leads to multidrug resistance in GBM cell lines [12]. Accordingly, a reduction of YAP/TAZ nuclear levels leads to the downregulation of downstream gene targets of the Hippo pathway.

The Hippo pathway may therefore represent a critical regulator of vasculogenic mimicry formation in GBM. Here, we assessed the pharmacological properties of three TEAD binders that target the Hippo pathway to reduce the expression of its downstream effectors CTGF, CYR61, AXL, and NF2. We further questioned whether such an approach would help circumvent vasculogenic mimicry–mediated chemoresistance in rare brain cancer disease.

Methods

Materials

SDS and BSA were purchased from Sigma-Aldrich Corp. (St Louis, Missouri, USA). Cell culture media Eagle's Minimum Essential Medium was from Wisent (320-005 CL) (Saint-Jean-Baptiste de Rouville, Quebec, Canada). Electrophoresis reagents were purchased from Bio-Rad Laboratories (Hercules, California, USA). The HyGLO Chemiluminescent horseradish peroxidase (HRP) Antibody Detection Reagents were from Denville Scientific Inc. (Metuchen, New Jersey, USA). Micro bicinchoninic acid (BCA) protein assay reagents were from Pierce (Micro BCA Protein Assay Kit; Thermo Fisher Scientific, Waltham, Massachusetts, USA). The polyclonal antibodies against Snail (3879S) as well as the mAb against glyceraldehyde 3-phosphate dehydrogenase (GAPDH) (D4C6R) were from Cell Signaling Technology (Danvers, Massachusetts, USA). The mAb against Fibrillarin (NB300-269) was purchased from Novus Biologicals (Toronto, Ontario, Canada). HRP-conjugated donkey anti-rabbit and anti-mouse immunoglobulin G secondary antibodies were from Jackson ImmunoResearch Laboratories (West Grove, Pennsylvania, USA).

Cell culture and capillary-like structure formation assay

The human U87 (HTB-14), U118 (HTB-15), U138 (HTB-16), and U251 GBM cell lines were from the American Type Culture Collection (ATCC, Manassas, Virginia, USA). They were all maintained in Eagle's Minimum Essential Medium (Wisent; 320-006CL) containing 10% (v/v) calf serum (HyClone Laboratories; SH30541.03, Logan, Utah, USA), 2 mmol/l glutamine, 1 mmol/l sodium pyruvate (Sigma-Aldrich, Oakville, Ontario, Canada; P2256), 100 U/ml penicillin and 100 mg/ml streptomycin (Wisent; 250-202-EL). Cells were incubated at 37 °C with 5% CO_2. Vasculogenic mimicry was assessed *in vitro* using Cultrex (3432-010-01; R&D Systems Inc.; Toronto, Ontario, Canada) to monitor three-dimensional capillary-like structure formation [23]. In brief, each well of a 96-well plate was precoated with 50 µl of Cultrex. Cell suspension in culture media (2×10^4 cells/100 µl) was then seeded on top of polymerized Cultrex. Tested compounds (HC258, LM41, and LM98) were added to the cell culture media at a 10 µmol/l concentration and incubated at 37 °C in a CO_2 incubator. Pictures were taken over time using a digital camera coupled to a phase-contrast inverted microscope. Mean loop area: For each loop, the area (number of pixels) enclosed by it is considered as its area. The mean loop area is the arithmetic mean of all loop areas. Mean loop perimeter: For each loop, the pixels that belong to its edge are considered its border or perimeter. The

Downloaded from http://journals.lww.com/anti-cancerdrugs by BhDMf5ePHKav1zEoum1tQfN4a+kJLhEZgbsIHo4XMi0hCywCX1AWnYQp/IlQrHD3i3D0OdRyi7TvSFl4Cf3VC4/OAVpDDa8K2+Ya6H515kE= on 07/02/2024

mean loop perimeter is the arithmetic mean of all loop perimeters. The number of loops and area covered upon tube branching formed by the cells were quantified using either the Wimasis Analysis Software (Cordoba, Spain) or the ImageJ software [24].

Total RNA isolation, cDNA synthesis, and real-time quantitative PCR

Total RNA was extracted from cell monolayers using 1 ml of TriZol reagent for a maximum of 3×10^6 cells as recommended by the manufacturer (Life Technologies, Gaithersburg, Maryland, USA). For cDNA synthesis, 1–2 µg of total RNA was reverse-transcribed using a high-capacity cDNA reverse transcription kit (Applied Biosystems, Foster City, California, USA) or, in the case of the gene array, an RT2 First Strand kit (QIAGEN, Valencia, California, USA). The cDNA was stored at –80 °C before PCR. Gene expression was quantified by real-time quantitative PCR (RT-qPCR) using iQ SYBR Green Supermix (Bio-Rad, Hercules, California, USA). DNA amplification was carried out using an Icycler iQ5 (Bio-Rad) and product detection was performed by measuring the binding of the fluorescent dye SYBR Green I to double-stranded DNA. The following primer sets were from QIAGEN: FOXC2 (Hs_FOXC2_1_SG, QT00220871), SNAI1 (Hs_SNAI1_1_SG, QT00010010), YAP1 (Hs_YAP1_1_SG, QT00080822), TEAD1 (Hs_TEAD1_1_SG, QT00000721), CTGF (Hs_CTGF_1_SG, QT00052899), CYR61 (Hs_CYR61_1_SG, QT00003451), AXL (Hs_AXL_1_SG, QT00067725), NF2 (Hs_NF2_va.1_SG, QT01004934), GAPDH (Hs_GAPDH_1_SG, QT00079247), and peptidylprolyl isomerase A (PPIA) (Hs_PPIA_4_SG, QT01866137). The relative quantities of target gene mRNA were normalized against internal housekeeping genes PPIA and GAPDH. The RNA was measured by following a ΔC_t method employing an amplification plot (fluorescence signal vs. cycle number). The difference (ΔC_t) between the mean values in the triplicate samples of the target gene and the housekeeping genes was calculated with the CFX manager Software, version 2.1 (Bio-Rad) and the relative quantified value was expressed as $2^{-\Delta Ct}$.

In-silico analysis of transcript levels in clinical glioblastoma and low-grade glioma tissues

A Gene Expression Profiling Interactive Analysis web server was used to analyze the RNA sequencing expression data of GBM tumors ($n = 163$) vs. healthy tissue ($n = 207$), and of low-grade glioma (LGG, $n = 518$) vs. healthy tissue ($n = 207$) from The Cancer Genome Atlas and the normal brain tissue in Genotype-Tissue Expression databases [25]. Gene Expression Profiling Interactive Analysis provides customizable functions such as tumor/normal differential expression analysis, profiling according to cancer types or pathological stages, patient survival analysis, similar gene detection, correlation analysis, and dimensionality reduction analysis (http://gepia.cancer-pku.cn/detail.php, accessed on 5 January 2024). One-way analysis of variance was used for differential analysis of gene expression, using disease states (GBM, LGG, or normal) as variables for the box plots.

TissueScan cDNA arrays of grades I–IV brain tumor tissues

TissueScan cancer and normal tissue cDNA arrays were purchased from OriGene (Rockville, Maryland, USA), covering 43 clinical samples of the four stages of brain cancer as well as normal tissues, and were used to assess *TEAD1*, *YAP1*, *CYR61*, and *CTGF* gene expression levels according to the manufacturer's recommendations. Tissue cDNAs in each array were synthesized from high-quality total RNAs of pathologist-verified tissues, normalized and validated with β-actin in two sequential quantitative PCR analyses, and accompanied by clinical information for 18 WHO defined grade I, 11 WHO grade II, 10 WHO grade III, and two WHO grade IV brain tumors.

Transfection method and RNA interference

For gene silencing experiments, U87 GBM cells were transiently transfected with small interfering RNA (siRNA) sequences using Lipofectamine-2000 transfection reagent (Thermo Fisher Scientific). Gene silencing was performed using 20 nmol/l siRNA against *CTGF* (FlexiTube siRNA, SI00029673), *CYR61* (FlexiTude siRNA, SI03028655), *SNAI1* (FlexiTube siRNA, SI00083398), *FOXC2* (FlexiTube siRNA, SI03090423), or scrambled sequences (AllStar Negative Control siRNA, 1027281). The above siRNA and mismatch siRNA were all synthesized by QIAGEN and annealed to form duplexes. Gene silencing efficacy was assessed by RT-qPCR as described above.

Real-time cell migration assay

Experiments were carried out using the Real-Time Cell Analyser Dual-Plate Instrument and the xCELLigence system (Roche Diagnostics, Laval, Quebec, Canada), following the instructions of the supplier. U87 cells were treated with vehicle (1% dimethyl sulfoxide) or 10 µmol/l LM98. $2{,}5 \times 10^4$ cells per well were seeded in a CIM-plate 16 (Roche Diagnostics) and incubated at 37 °C under a humidified atmosphere containing 5% CO_2 for 24 h. Before cell seeding, the underside of each well in the upper chamber was coated with 0.15% gelatin in PBS and incubated for 1 h at 37 °C. The lower chamber wells were filled with serum-free medium. After 30 min of adhesion, cell migration was monitored every 5 min for 6 h. The impedance value was measured by the Real-Time Cell Analyser Dual-Plate Instrument and expressed as an arbitrary unit called the Cell Index. Each experiment was performed in quadruplicate wells.

Fig. 1

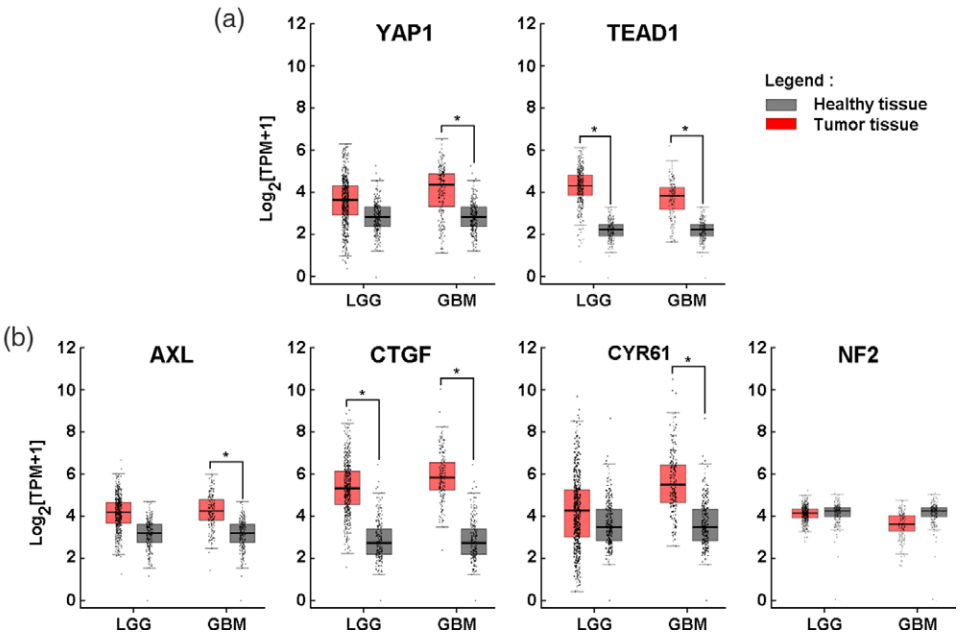

Increased gene expression of *YAP1*, *TEAD1*, and downstream effectors *AXL*, *CTGF*, and *CYR61 in* clinically annotated glioblastoma tumor tissues. In-silico analysis of transcript levels was performed using RNA extracted from clinical samples from glioblastoma (GBM) and low-grade glioma (LGG) (red boxes) and compared with healthy tissue (gray boxes) (*$P < 0.05$).

Protein–protein interaction

The associative relationships of YAP/TEAD and of downstream effectors were retrieved from the STRING, v11 database (https://www.string-db.org/) to identify and build protein–protein interaction networks [26], with a confidence score setting of 0.4, and the maximum number of interactions to show was no more than 10.

Nuclear extraction

Cell monolayers were first lysed with a cytoplasmic buffer and then with a nuclear buffer according to the manufacturer's instructions (Invent Biotechnologies; Plymouth, Minnesota, USA, SC-003). In the case of cells cultured on Cultrex, they were first detached from the matrix using a nonenzymatic Cultrex organoid harvesting and dissociation solution (3700-100-01; R&D Systems Inc.).

Western blot

Cells and nuclear fractions, isolated as described above, were lysed in a buffer containing 1 mmol/l each of sodium fluoride and sodium orthovanadate. Proteins (10–20 µg) were then separated by SDS-polyacrylamide gel electrophoresis. Next, proteins were electrotransferred to low-fluorescence polyvinylidene difluoride membranes and blocked for 1 h at room temperature with 5% nonfat dry milk in Tris-buffered saline (150 mmol/l NaCl, 20 mmol/l Tris-HCl, pH 7.5) containing 0.3% Tween-20 (TBST; Bioshop, Burlington, Ontario, Canada, TWN510-500). Membranes were washed in TBST and incubated overnight with the appropriate primary antibodies (1/1000 dilution) in TBST containing 3% BSA and 0.1% sodium azide (Sigma-Aldrich, Oakville, Ontario, Canada) at 4 °C and on a shaker. After three washes with TBST, the membranes were incubated for 1 h with HRP-conjugated anti-rabbit or anti-mouse immunoglobulin G at 1/2500 dilutions in TBST containing 5% nonfat dry milk. Immunoreactive material was visualized by enhanced chemiluminescence.

Statistical data analysis

Data and error bars were expressed as mean ± SEM of three or more independent experiments unless otherwise stated. Hypothesis testing was conducted using the Kruskal–Wallis test followed by a Dunn Tukey's post-test (data with more than three groups) or a Mann–Whitney test (two-group comparisons). Probability (P) values of less than 0.05 (*) were considered significant and denoted in the figures. All statistical analyses were performed using the GraphPad Prism 7 software (GraphPad Software LLC, San Diego, California, USA).

Results

High transcripts expression of the Hippo signaling pathway mediators in clinically annotated glioblastoma tissues

Transcript levels from 518 clinically annotated LGG and 163 GBM tissues were retrieved from The Cancer

Downloaded from http://journals.lww.com/anti-cancerdrugs by BhDMf5ePHKav1zEoum1tQfN4a+kJLhEZgbsIHo4XMi0hCywCX1AWnYQp/IlQrHD3i3D0OdRyi7TvSFl4Cf3VC4/OAVpDDa8K2+Ya6H515kE= on 07/02/2024

Downloaded from http://journals.lww.com/anti-cancerdrugs by BhDMf5ePHKav1zEoum1tQfN4a+kJLhEZgbsIHo4XMi0hCywCX1AWnYQp/IlQrHD3i3D0OdRyi7TvSFl4Cf3VC4/OAVpDDa8K2+Ya6H515kE= on 07/02/2024

Fig. 2

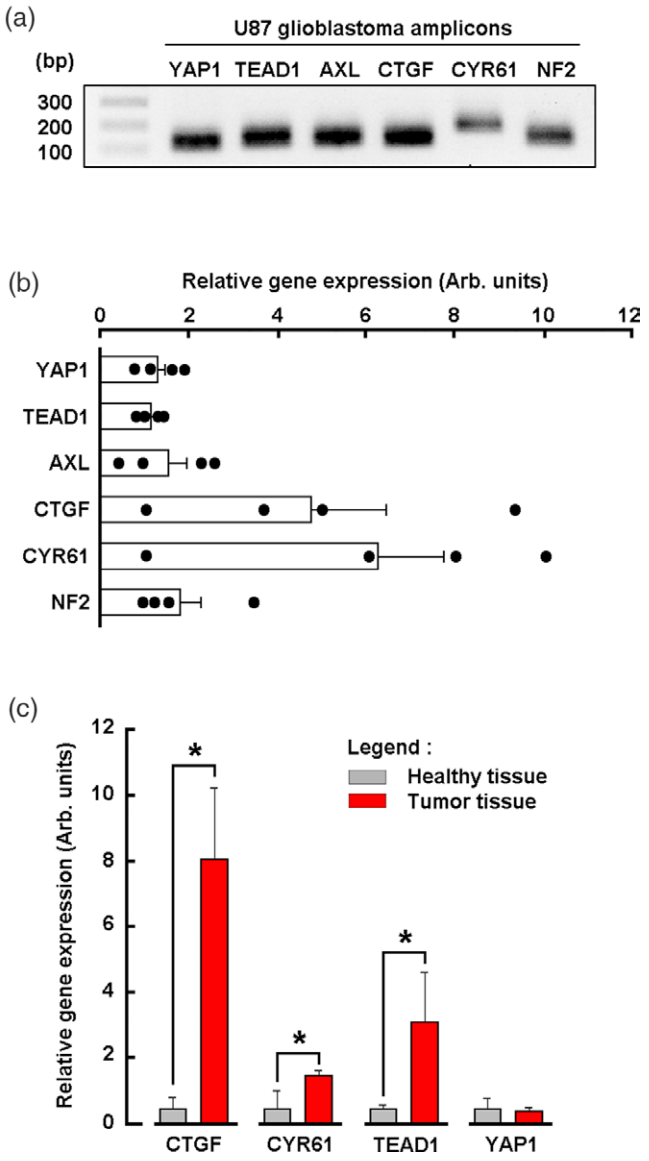

Expression profiles of *YAP1*, *TEAD1*, *AXL*, *CTGF*, *CYR61*, and NF2 in four human glioblastoma cell lines, and in cDNA tissue arrays. Total RNA was extracted from four different human glioblastoma cell lines (U87, U118, U251, and U138). The gene expression level for *YAP1*, *TEAD1*, *AXL*, *CTGF*, *CYR61*, and *NF2* was analyzed and compared by real-time quantitative PCR. (a) Primer validation and single amplicon products were confirmed using agarose gel electrophoresis for the U87 cell line. (b) The gene expression levels of the six selected genes were analyzed and quantified by quantitative PCR as described in the Methods section. Triplicates from a representative quantification, out of three independent experiments, are shown. (c) Cancer tissues (red boxes) and normal tissues (gray boxes) cDNA arrays covering 43 clinical samples of the pooled four stages of pathologist-verified brain cancer tissues as well as normal tissues were screened to assess *TEAD1*, *YAP1*, *CYR61*, and *CTGF* gene expression levels by quantitative PCR. *$P < 0.05$.

Genome Atlas and the normal brain tissue in Genotype-Tissue Expression databases and compared with 207 healthy tissues. *YAP1* and *TEAD1* transcript levels were found to be increased in GBM tissues (Fig. 1a) and this was indicative of a potential increase in their downstream effectors. When assessed, *CYR61*, *CTGF*, and *AXL* transcripts were effectively increased whereas *NF2* remained unchanged (Fig. 1b). Interestingly, only *TEAD1* and *CTGF* transcripts were found induced in LGG. This observation confirms the activation of the Hippo pathway and downstream signaling intermediates in GBM.

Human glioblastoma cell line models and glioblastoma clinical samples recapitulate the high expression levels of *CYR61* and *CTGF* transcripts

The expression of the Hippo signaling pathway members was assessed in-vitro in four different human GBM cell line models namely U87, U118, U138, and U251, along with several of their downstream effectors using RT-qPCR. Total RNA was extracted from cell monolayers, cDNA was generated, and the presence of a single amplicon was validated for all of them. For the sake of clarity, only amplicons from U87 GBM cells are shown here (Fig. 2a). Collectively, basal *CYR61* and *CTGF* transcript levels were found to be significantly increased whereas they remained low for all the other genes tested (Fig. 2b). Lower expressions, however, do not preclude that they could still be higher than their normal healthy tissues. Cancer and normal tissue cDNA arrays, covering 43 clinical samples of the four stages of pathologist-verified brain cancer tissues as well as normal tissues, were screened to assess *TEAD1*, *YAP1*, *CYR61*, and *CTGF* gene expression levels by quantitative PCR. Tissue arrays further confirmed the differentially increased tendencies for *TEAD1*, *CTGF*, and *CYR61* expression in tumor tissues (Fig. 2c, red boxes) when compared with their healthy tissue (Fig. 2c, gray boxes). YAP1 was not found to vary between the healthy and tumor tissues.

Increased *CYR61* and *CTGF* transcriptional regulation in U87 glioblastoma cells upon in-vitro vasculogenic mimicry

Four different human GBM cell line models were next tested for their capacity to form in-vitro vasculogenic mimicry. U118, U138, U251, and U87 GBM cells were seeded either on plastic as two-dimensional monolayers or on Cultrex, as described in the Methods section, to generate three-dimensional structures. Defined three-dimensional capillary-like structures were formed with U87 cells, whereas U251, U118, and U138 cells were either too proliferative or did not form structures within our experimental conditions (Fig. 3a). When total RNA was extracted from U87 cell cultures and processed for gene analysis by RT-qPCR, *CTGF* and *CYR61* were found induced upon vasculogenic mimicry when compared with two-dimensional monolayers (Fig. 3b). Vasculogenic mimicry kinetic was also performed using U87 cells, and three-dimensional structures were found to mature upon

Fig. 3

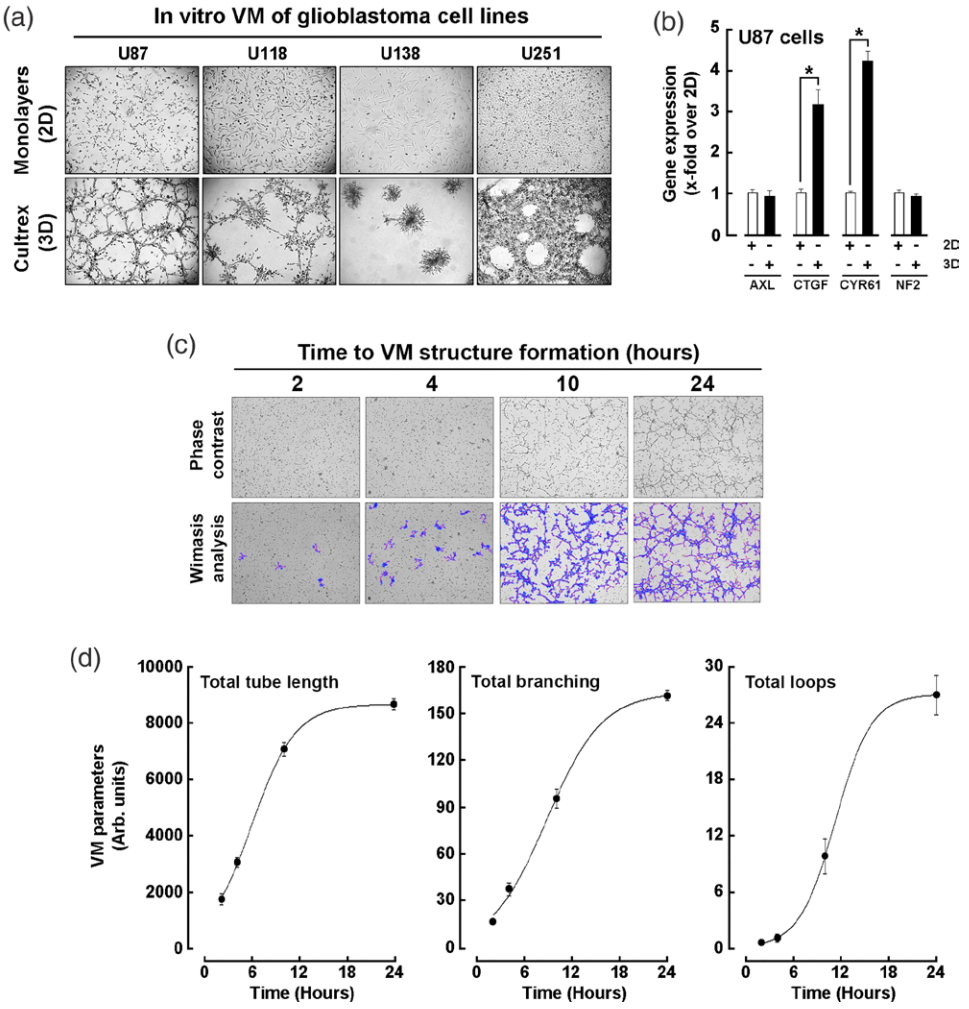

In-vitro human glioblastoma cell lines, capillary-like structure formation on Cultrex. Cells were trypsinized and seeded on top of Cultrex to generate three-dimensional capillary-like structures as described in the Methods section. (a) Representative phase-contrast pictures were taken to monitor structure formation at 24 h in U87, U118, U138, and U251 (×4 magnification). (b) *CYR61* and *CTGF* levels are induced in in-vitro vasculogenic mimicry (VM) of the human U87 glioblastoma cell line. Total RNA was extracted either from cells cultured on Cultrex (black bars) or cells cultured as two-dimensional adherent monolayers (white bars). Real-time quantitative PCR analysis was next used to study the expression of the Hippo pathway downstream effectors. (c) Representative phase-contrast pictures were taken (upper panels), and Wimasis analysis of the structures represented in blue (lower panels). (d) VM parameters were extracted from the Wimasis analysis of (c) and representative quantification provided for total tube length, total branching, or total loops. *$P < 0.05$.

10–24 h (Fig. 3c), with increasing vasculogenic mimicry parameters assessed using Wimasis which included total tube length, branching, and loops (Fig. 3d).

Small interfering RNA–mediated repression of *CYR61* and *CTGF* inhibits U87 glioblastoma cells vasculogenic mimicry

To assess the impact of CTGF and CYR61 on vasculogenic mimicry, transient gene silencing was performed to specifically repress both genes and this was validated by quantitative PCR (Fig. 4a). Cells were next seeded on top of Cultrex, and three-dimensional structures found to be significantly altered as compared with control cells (siScrambled, Fig. 4b). Vasculogenic mimicry parameters of tube length, branching points, and loops were accordingly reduced (Fig. 4c).

Protein–protein interaction network predicts YAP-TEAD interrelationship with downstream biomarkers involved in the Hippo pathway and in epithelial-to-mesenchymal transition during U87 capillary-like structure formation

A protein–protein interaction network of YAP-TEAD was constructed using the STRING database (https://string-db.org/) and was used to predict and analyze potential YAP-TEAD interactors. Indirect target proteins were retrieved from STRING as described in the Methods section. The network predicted YAP/TEAD inter-relationship with biomarkers involved in

Downloaded from http://journals.lww.com/anti-cancerdrugs by BhDMf5ePHKav1zEoum1tQfN4a+kJLhEZgbsIHo4XMi0hCywCX1AWnYQp/IlQrHD3i3D0OdRyi7TvSFl4Cf3VC4/OAVpDDa8K2+Ya6H515kE= on 07/02/2024

Downloaded from http://journals.lww.com/anti-cancerdrugs by BhDMf5ePHKav1zEoum1tQfN4a+kJLhEZgbsIHo4XMi0hCywCX1AWnYQp/IlQrHD3i3D0OdRyi7TvSFl4Cf3VC4/OAVpDDa8K2+Ya6H515kE= on 07/02/2024

Fig. 4

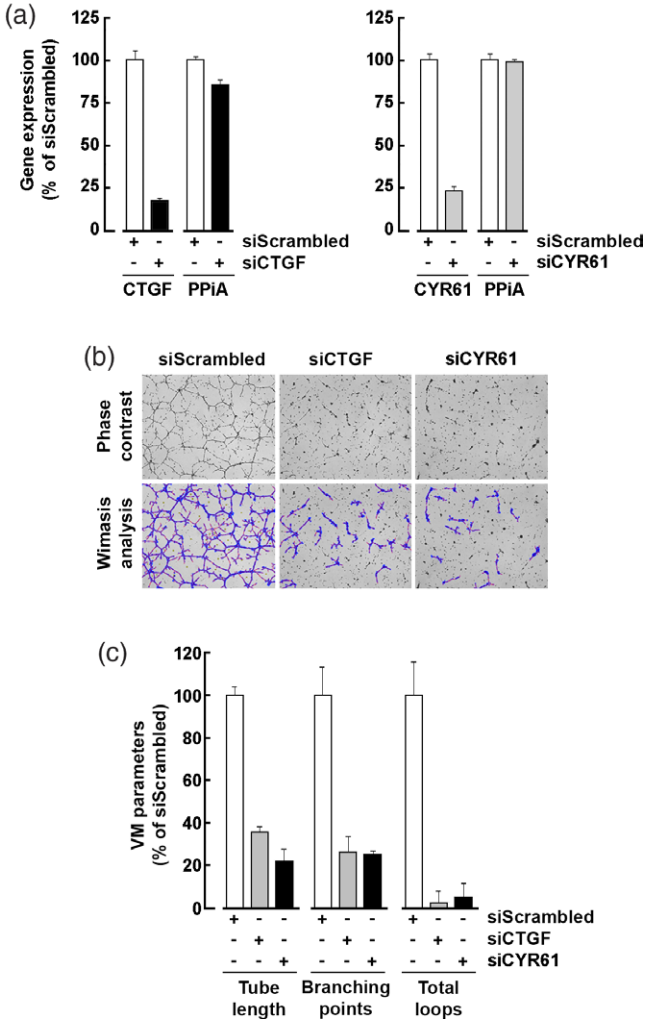

Silencing of CTGF or CYR61 alters the U87 capillary-like structure formation. (a) U87 glioblastoma cell monolayers were transiently transfected with a scrambled sequence (siScrambled) or a small interfering RNA (siRNA) directed against *CTGF* (siCTGF) or *CYR61* (siCYR61). Total RNA was then extracted, and gene silencing efficiency was validated using real-time quantitative PCR. Gene levels were normalized on glyceraldehyde 3-phosphate dehydrogenase expression. (b) Transfected U87 cells were seeded on top of Cultrex, and three-dimensional capillary-like structures were generated for 24 h. Representative phase-contrast pictures were taken (upper panels) and Wimasis analysis (lower panels) was performed. (c) Vasculogenic mimicry parameters were extracted from the Wimasis analysis of (b) and representative quantification was provided for total tube length, total branching points, or total loops. PPiA, peptidylprolyl isomerase A.

epithelial-to-mesenchymal transition (EMT) such as FOXC2 and Snail (Fig. 5a). Upon U87 capillary-like structure formation, total RNA was extracted from triplicate samples and three-dimensional vs. two-dimensional culture conditions compared the gene expression modulation using RT-qPCR as described in the Methods section. *FOXC2* and *SNAI1* gene expression levels were found to increase in three-dimensional structures (Fig. 5b).

Silencing of *SNAI1* or *FOXC2* alters the U87 capillary-like structure formation

U87 GBM cell monolayers were transiently transfected with either a scrambled sequence (Fig. 6a, white bars), a siRNA directed against *SNAI1* (Fig. 6a, gray bars), or against *FOXC2* (Fig. 6a, black bars). Total RNA was next extracted, and gene silencing efficiency was validated using RT-qPCR. Transient gene silencing of *SNAI1* or *FOXC2* effectively reduced *CTGF* and *CYR61* gene expression. When the respective transfected cells were seeded on top of Cultrex three-dimensional, capillary-like structures generated upon 24 h were found reduced when *SNAI1* and *FOXC2* were silenced. This suggests that *CTGF* and *CYR61* exert a regulatory function in vasculogenic mimicry.

Hippo pathway pharmacological targeting alters U87 capillary-like structure formation and nuclear expression of Snail

Recent pharmacological inhibitors of the Hippo signaling pathway were tested for their capacity to target vasculogenic mimicry. These included HC258, LM41, and LM98 molecules (Fig. 7a) [7–9]. Vasculogenic mimicry was found to be inhibited only by LM98 (Fig. 7b) as it reduced tube length, branching points, and loops (Fig.7c, black bars). Interestingly, LM98 was able to reduce *CTGF*, *CYR61*, *FOXC2*, and *SNAI1* transcript levels from three-dimensional cultures (Fig. 7d), as well as chemotaxis assessed by real-time xCELLigence (Fig. 7e). When nuclear fractionation was assessed upon vasculogenic mimicry in basal conditions, Snail was significantly found to translocate within the nuclear fraction (Fig. 7f, upper panel). LM98 treatment significantly reduced such Snail translocation. Fibrillarin expression in the nucleus and GAPDH expression in the cytosolic fraction validate the fractionation procedure.

Discussion

Therapeutic targeting strategies of the YAP/TEAD transcriptional complex have recently emerged as it is responsible for the expression of genes that regulate cancer cell growth, and proliferation [27]. For instance, the recent design, synthesis, and biological evaluation of LM98, a flufenamic acid (FA) analog with a strong affinity to TEAD and a capacity to inhibit its autopalmitoylation, was able to reduce the YAP/TEAD transcriptional activity [9]. Interestingly, LM98's capacity to reduce the *CTGF* and *CYR61* transcript levels was also correlated with the inhibition of MDA-MB-231 breast cancer cell migration and proliferation through the arrest of the cell cycle [9]. Taken together, developing strategies to block the formation of the YAP/TEAD transcription complex therefore appeared as a plausible initial pharmacological approach to abolish the oncogenic function of YAP [28]. In addition, the silencing of most YAP-inducible genes and attenuation of YAP-induced overgrowth in

Fig. 5

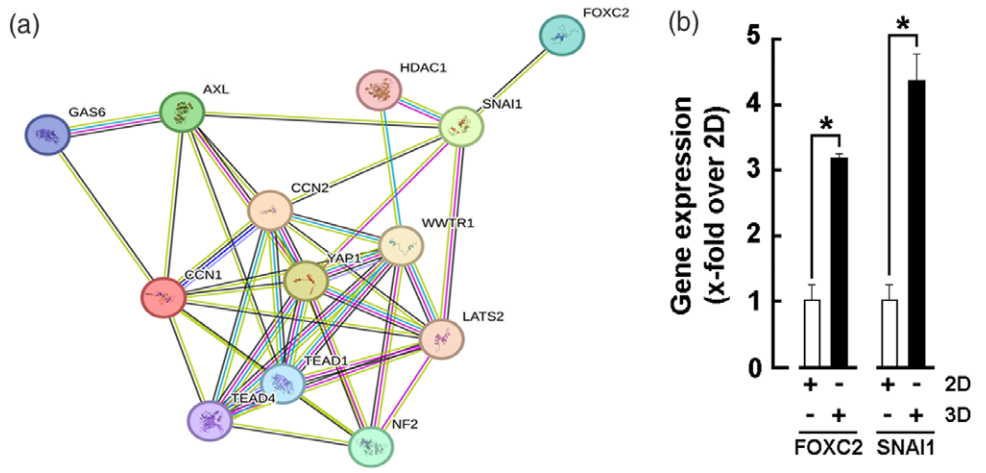

Transcriptomic analysis reveals that SNAI1 and FOXC2 expression levels are induced in U87 capillary-like structure formation. (a) Indirect target proteins of YAP1 were retrieved from STRING as described in the Methods section. (b) Human U87 glioblastoma cells were seeded as either two-dimensional (2D) monolayers (2D, white bars) or as three-dimensional (3D) capillary-like structures on top of Cultrex (3D, black bars) for 24 h. Total RNA was extracted from triplicate samples for each condition, and gene expression modulation for two of the predicted targets (FOXC2 and Snail) was assessed by real-time quantitative PCR as described in the Methods section. *$P < 0.05$.

Fig. 6

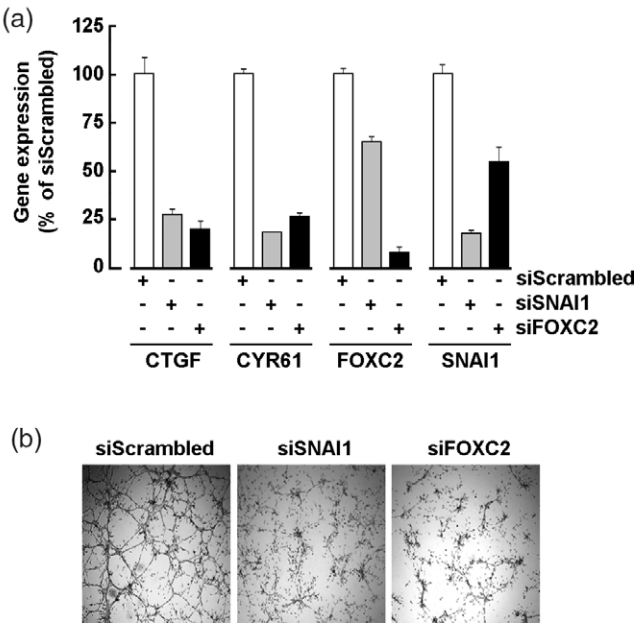

Silencing of SNAI1 or FOXC2 alters the U87 capillary-like structure formation. (a) U87 glioblastoma cell monolayers were transiently transfected with a scrambled sequence (siScrambled, white bars) or small interfering RNA (siRNA) directed against *SNAI1* (siSNAI1, gray bars) or *FOXC2* (siFOXC2, black bars). Total RNA was then extracted, and gene silencing efficiency was validated using real-time quantitative PCR. (b) Transfected U87 cells were seeded on top of Cultrex and three-dimensional capillary-like structures were generated for 24 h. Representative phase-contrast pictures were taken.

TEAD knockdown further confirmed the validity of the Hippo pathway as a target for drug discovery [29]. While we report herein that transcript levels of *CTGF* and *CYR61* downstream effectors of the Hippo pathway were increased in clinically annotated human GBM samples, and significantly induced upon in-vitro vasculogenic mimicry in the U87 grade IV GBM-derived brain cancer cell model, the impact of new small molecules targeting the Hippo pathway remains to be assessed.

Several TEAD inhibitors, among which LM98, a reversible TEAD inhibitor that originates from the fusion of flufenamic acid and palmitic acid, were previously reported by us to alter breast cancer cell migration [7–9]. Here, only LM98 appeared to specifically inhibit in-vitro vasculogenic mimicry in U87 GBM cells. In fact, HC258, a covalent acrylamide TEAD inhibitor that also reduced gene expression and cell migration [8], as well as LM41, an flufenamic acid–derived TEAD inhibitor obtained through the replacement of its trifluoromethyl group by aryl rings [7], were tested alongside LM98, but found ineffective to inhibit in-vitro vasculogenic mimicry in our experimental settings. HC258 is derived from flufenamic acid and possesses an oxopentyl chain that mimics a molecule of palmitic acid as well as an acrylamide that reacts covalently with TEAD's cysteine. While such derivative appeared to alter YAP/TEAD mediated transcriptional activity, the differential structure-to-function impact of those molecules on in-vitro vasculogenic mimicry suggests that specific and more complex interplay links the Hippo pathway to ECM recognition processes that regulate vasculogenic mimicry, and this warrants further molecular investigation.

The proto-oncogenic nature of YAP comes from its interaction with TEAD leading to the activation of genes that confer chemoresistance and metastasis-associated traits to transformed cells [30]. In GBM, the overexpression of

Downloaded from http://journals.lww.com/anti-cancerdrugs by BhDMf5ePHKav1zEoum1tQfN4a+kJLhEZgbsIHo4XMi0hCywCX1AWnYQp/IlQrHD3i3D0OdRyi7TvSFl4Cf3VC4/OAVpDDa8K2+Ya6H515kE= on 07/02/2024

Fig. 7

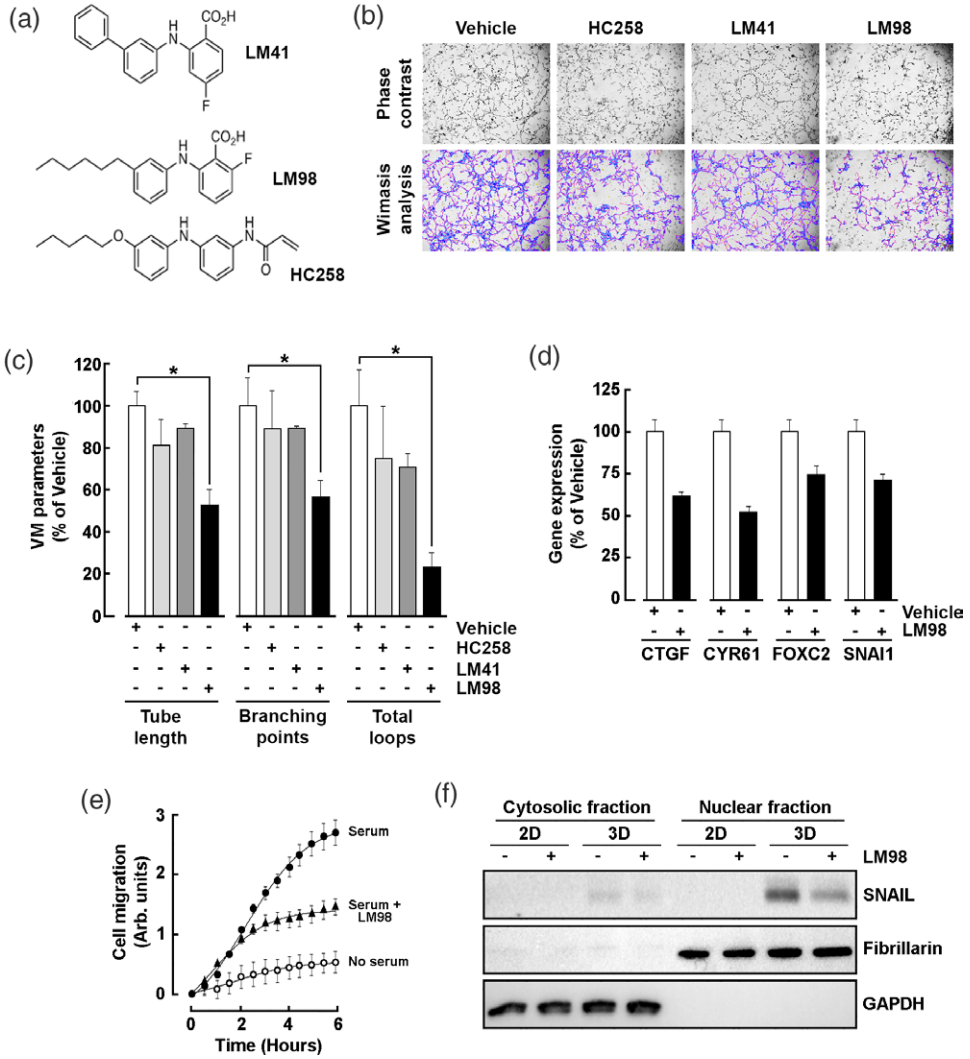

Hippo pathway pharmacological targeting alters U87 capillary-like structure formation and nuclear expression of *SNAI1*. (a) Chemical structure of the tested TEAD inhibitors. (b) Human U87 glioblastoma cells were seeded on top of Cultrex and three-dimensional capillary-like structures were generated for 24 h in the absence (vehicle) or presence of 10 μmol/l Hippo inhibitors HC258, LM41, and LM98, respectively. Representative phase-contrast pictures were taken (upper panels) and Wimasis analysis (lower panels) was performed. (c) Vasculogenic mimicry (VM) parameters were extracted from the Wimasis analysis of (b) and representative quantification was provided for total tube length, branching points, or total loops. (d) The effect of compound LM98 on *CTGF*, *CYR61*, *FOXC2*, and *SNAI1* gene expression was assessed by real-time quantitative PCR as described in the Methods section. LM98-treated (black bars) or nontreated (white bars) U87 glioblastoma cells were seeded as three-dimensional capillary-like structures on top of Cultrex for 24 h. Total RNA was extracted from triplicate samples for each condition. (e) Real-time cell migration was assessed using the xCELLigence as described in the Methods section. (f) Nuclear fractionation protocol was performed from two-dimensional or three-dimensional U87 treated or not with LM98. Total proteins were extracted and representative blots for Snail, Fibrillarin, and glyceraldehyde 3-phosphate dehydrogenase (GAPDH) are presented. Western blotting of nuclear fibrillarin enrichment and undetectable contamination from cytosolic GAPDH. $^*P < 0.05$.

the YAP/TAZ-TEAD complex induces cell resistance to temozolomide treatment by upregulation of the Hippo pathway downstream target genes [12]. Interestingly, *CTGF* and *CYR61* genes were found upregulated through transforming growth factor (TGF) β1-dependent activation of Smad/ERK signaling [31], an event that triggers the expression and nuclear translocation of Snail upon EMT in GBM by TGFβ1 [32,33], and which is induced upon in-vitro vasculogenic mimicry herein. Accordingly, we demonstrated that LM98 inhibited both *SNAI1* transcript levels and Snail translocation to the nucleus and that specific transient siRNA-mediated repression of *SNAI1* abolished in-vitro vasculogenic mimicry. TGFβ signaling pathway regulates two distinct aspects of vasculogenic mimicry formation involving the maintenance of the undifferentiated embryonic state of stem cells via EMT, and the induction of tubular formation through modulation of the tumor microenvironment [15]. High

Downloaded from http://journals.lww.com/anti-cancerdrugs by BhDMf5ePHKav1zEoum1tQfN4a+kJLhEZgbsIHo4XMi0hCywCX1AWnYQp/IlQrHD3i3D0OdRyi7TvSFl4Cf3VC4/OAVpDDa8K2+Ya6H515kE= on 07/02/2024

Downloaded from http://journals.lww.com/anti-cancerdrugs by BhDMf5ePHKav1zEoum1tQfN4a+kJLhEZgbsIHo4XMi0hCywCX1AWnYQp/IlQrHD3i3D0OdRyi7TvSFl4Cf3VC4/OAVpDDa8K2+Ya6H515kE= on 07/02/2024

expression of Snail appeared to link vasculogenic mimicry to TGF-β1 treatment in ovarian cancer cells, and this was efficiently repressed by diet-derived gallated catechins [34]. In fact, targeting vasculogenic mimicry by phytochemicals is envisioned as a potential opportunity for cancer therapy [35]. This further lays the foundation for the potential repurposing of molecules such as verteporfin, an antitumor drug in the treatment of pancreatic cancer by targeting the Hippo pathway which was recently found to also inhibit in-vitro vasculogenic mimicry [36].

Conclusion

Recent advancements in medicinal chemistry such as the development of LM98, a potent TEAD inhibitor, have demonstrated promising results in inhibiting YAP/TEAD transcriptional activity, altering in-vitro vasculogenic mimicry, and reducing cancer cell migration. Our study highlights the potential of Hippo pathway targeting in cancer therapy and pave the way for future investigation into its underlying mechanisms. Several molecules have been developed for the treatment of GBM and have been granted the designation of orphan drugs by the FDA or EMA. Many of these molecules, however, have not been approved for marketing or have shown limited efficacy during clinical trials primarily because of their inability to target the chemoresistance phenotype of these rare brain cancers. Therefore, there is a high unmet need for new therapeutic strategies for GBM patients. Our current study therefore aimed to explore the preclinical pharmacological impact of new small-molecule YAP/TEAD inhibitors against vasculogenic mimicry processes. As vasculogenic mimicry can be induced by numerous factors in GBM, such as hypoxia, inflammation, growth factors, and extracellular matrix components, it can also vary depending on the tumor microenvironment and stage. Hence, diagnosing vasculogenic mimicry and treating vasculogenic mimicry–related processes in GBM is a considerable challenge. Our current innovative medicinal chemistry strategy may therefore offer new opportunities for improving the prognosis and quality of life of GBM patients.

Acknowledgements

Conceptualization: M.-E.R. and B.A.; data curation: M.-E.R. and C.V.; formal analysis and writing – original draft: M.-E.R., A.G., and B.A.; funding acquisition: A.G. and B.A.; investigation: M.-E.R., C.V., and A.P.; methodology: M.-E.R. and A.P.; supervision: B.A. and A.G.; writing – review and editing: M.-E.R., C.V., A.P., A.G., and B.A. All authors read and approved the final manuscript.

This work was funded by the Institutional Research Chair in Cancer Prevention and Treatment held by Dr Borhane Annabi at UQAM, and by a Fonds de Recherche du Québec – Nature et Technologie (FRQNT) team grant between A.G. and B.A. A.G. is the holder of an Institutional Chair in Epigenetics and Medicinal Chemistry at UQAM. C.V. holds a Natural Sciences and Engineering Research Council of Canada (NSERC) and FRQNT Fellowship. A.P. holds a Réseau Québécois de la Recherche sur le Médicament (RQRM), an NSERC, and an FRQNT Fellowship.

All data generated or analyzed during this study are included in this published article.

Conflicts of interest

There are no conflicts of interest.

References

1 GARD (Genetic and Rare Diseases Information Center). https://rarediseases.info.nih.gov/diseases/2491/glioblastoma. [Accessed 14 May 2024]
2 Lassen U, Mau-Sørensen M, Skovgaard Poulsen H. Orphan drugs in glioblastoma multiforme: a review. *Orphan Drugs Res Rev* 2014; **4**:83–91.
3 Mariz S, Reese JH, Westermark K, Greene L, Goto T, Hoshino T, *et al*. Worldwide collaboration for orphan drug designation. *Nat Rev Drug Discov* 2016; **15**:440–441.
4 Di Nunno V, Franceschi E, Tosoni A, Di Battista M, Gatto L, Lamperini C, *et al*. Treatment of recurrent glioblastoma: state-of-the-art and future perspectives. *Expert Rev Anticancer Ther* 2020; **20**:785–795.
5 Agosti E, Zeppieri M, De Maria L, Tedeschi C, Fontanella MM, Panciani PP, *et al*. Glioblastoma immunotherapy: a systematic review of the present strategies and prospects for advancements. *Int J Mol Sci* 2023; **24**:15037.
6 Himes BT, Geiger PA, Ayasoufi K, Bhargav AG, Brown DA, Parney IF. Immunosuppression in glioblastoma: current understanding and therapeutic implications. *Front Oncol* 2021; **11**:770561.
7 Fnaiche A, Melin L, Suárez NG, Paquin A, Vu V, Li F, *et al*. Development of LM-41 and AF-2112, two flufenamic acid-derived TEAD inhibitors obtained through the replacement of the trifluoromethyl group by aryl rings. *Bioorg Med Chem Lett* 2023; **95**:129488.
8 Fnaiche A, Chan HC, Paquin A, González Suárez N, Vu V, Li F, *et al*. Development of HC-258, a covalent acrylamide TEAD inhibitor that reduces gene expression and cell migration. *ACS Med Chem Lett* 2023; **14**:1746–1753.
9 Mélin L, Abdullayev S, Fnaiche A, Vu V, González Suárez N, Zeng H, *et al*. Development of LM98, a small-molecule TEAD inhibitor derived from flufenamic acid. *ChemMedChem* 2021; **16**:2982–3002.
10 Masliantsev K, Karayan-Tapon L, Guichet PO. Hippo signaling pathway in gliomas. *Cells* 2021; **10**:184.
11 Han Y. Analysis of the role of the Hippo pathway in cancer. *J Transl Med* 2019; **17**:116.
12 Casati G, Giunti L, Iorio AL, Marturano A, Galli L, Sardi I. Hippo pathway in regulating drug resistance of glioblastoma. *Int J Mol Sci* 2021; **22**:13431.
13 Ouyang T, Meng W, Li M, Hong T, Zhang N. Recent advances of the Hippo/YAP signaling pathway in brain development and glioma. *Cell Mol Neurobiol* 2020; **40**:495–510.
14 Fu M, Hu Y, Lan T, Guan KL, Luo T, Luo M. The Hippo signalling pathway and its implications in human health and diseases. *Signal Transduct Target Ther* 2022; **7**:376. Erratum in: Signal Transduct Target Ther. 2024; 9(1):5.
15 Mao JM, Liu J, Guo G, Mao XG, Li CX. Glioblastoma vasculogenic mimicry: signaling pathways progression and potential anti-angiogenesis targets. *Biomark Res* 2015; **3**:8.
16 Qiao K, Liu Y, Xu Z, Zhang H, Zhang H, Zhang C, *et al*. RNA m6A methylation promotes the formation of vasculogenic mimicry in hepatocellular carcinoma via Hippo pathway. *Angiogenesis* 2021; **24**:83–96. Erratum in: Angiogenesis. 2023; 26(1):197–199.
17 Zhang Y, Bai J, Cheng R, Zhang D, Qiu Z, Liu T, *et al*. TAZ promotes vasculogenic mimicry in gastric cancer through the upregulation of TEAD4. *J Gastroenterol Hepatol* 2022; **37**:714–726.
18 He PC, He C. m6 A RNA methylation: from mechanisms to therapeutic potential. *EMBO J* 2021; **40**:e105977.
19 Emami Nejad A, Najafgholian S, Rostami A, Sistani A, Shojaeifar S, Esparvarinha M, *et al*. The role of hypoxia in the tumor microenvironment and development of cancer stem cell: a novel approach to developing treatment. *Cancer Cell Int* 2021; **21**:62.

20 Chang HA, Ou Yang RZ, Su JM, Nguyen TMH, Sung JM, Tang MJ, *et al*. YAP nuclear translocation induced by HIF-1α prevents DNA damage under hypoxic conditions. *Cell Death Discov* 2023; **9**:385.
21 Zhou X, Lei QY. Regulation of TAZ in cancer. *Protein Cell* 2016; **7**:548–561.
22 Bhat KP, Salazar KL, Balasubramaniyan V, Wani K, Heathcock L, Hollingsworth F, *et al*. The transcriptional coactivator TAZ regulates mesenchymal differentiation in malignant glioma. *Genes Dev* 2011; **25**:2594–2609.
23 Uthamacumaran A, Suarez NG, Baniré Diallo A, Annabi B. Computational methods for structure-to-function analysis of diet-derived catechins-mediated targeting of in vitro vasculogenic mimicry. *Cancer Inform* 2021; **20**:11769351211009229.
24 Schneider CA, Rasband WS, Eliceiri KW. NIH Image to ImageJ: 25 years of image analysis. *Nat Methods* 2012; **9**:671–675.
25 Tang Z, Li C, Kang B, Gao G, Li C, Zhang Z. GEPIA: a web server for cancer and normal gene expression profiling and interactive analyses. *Nucleic Acids Res* 2017; **45**:W98–W102.
26 Szklarczyk D, Gable AL, Nastou KC, Lyon D, Kirsch R, Pyysalo S, *et al*. The STRING database in 2021: customizable protein-protein networks, and functional characterization of user-uploaded gene/measurement sets. *Nucleic Acids Res* 2021; **49**:D605–D612. Erratum in: Nucleic Acids Res. 2021; 49(18):10800.
27 Cunningham R, Hansen CG. The Hippo pathway in cancer: YAP/TAZ and TEAD as therapeutic targets in cancer. *Clin Sci (Lond)* 2022; **136**:197–222.
28 Zhao B, Kim J, Ye X, Lai ZC, Guan KL. Both TEAD-binding and WW domains are required for the growth stimulation and oncogenic transformation activity of yes-associated protein. *Cancer Res* 2009; **69**:1089–1098.
29 Dey A, Varelas X, Guan KL. Targeting the Hippo pathway in cancer, fibrosis, wound healing and regenerative medicine. *Nat Rev Drug Discov* 2020; **19**:480–494.
30 Luo J, Zou H, Guo Y, Tong T, Chen Y, Xiao Y, *et al*. The oncogenic roles and clinical implications of YAP/TAZ in breast cancer. *Br J Cancer* 2023; **128**:1611–1624.
31 Zeng H, Yang Z, Xu N, Liu B, Fu Z, Lian C, *et al*. Connective tissue growth factor promotes temozolomide resistance in glioblastoma through TGF-β1-dependent activation of Smad/ERK signaling. *Cell Death Dis* 2017; **8**:e2885.
32 Djediai S, Gonzalez Suarez N, El Cheikh-Hussein L, Rodriguez Torres S, Gresseau L, Dhayne S, *et al*. MT1-MMP cooperates with TGF-β receptor-mediated signaling to trigger SNAIL and induce epithelial-to-mesenchymal-like transition in U87 glioblastoma cells. *Int J Mol Sci* 2021; **22**:13006.
33 Torabidastgerdooei S, Roy ME, Annabi B. A molecular signature for the G6PC3/SLC37A2/SLC37A4 interactors in glioblastoma disease progression and in the acquisition of a brain cancer stem cell phenotype. *Front Endocrinol (Lausanne)* 2023; **14**:1265698.
34 Sicard AA, Dao T, Suarez NG, Annabi B. Diet-derived gallated catechins prevent TGF-β-mediated epithelial-mesenchymal transition, cell migration and vasculogenic mimicry in chemosensitive ES-2 ovarian cancer cells. *Nutr Cancer* 2021; **73**:169–180.
35 Haiaty S, Rashidi MR, Akbarzadeh M, Maroufi NF, Yousefi B, Nouri M. Targeting vasculogenic mimicry by phytochemicals: a potential opportunity for cancer therapy. *IUBMB Life* 2020; **72**:825–841.
36 Wei H, Wang F, Wang Y, Li T, Xiu P, Zhong J, *et al*. Verteporfin suppresses cell survival, angiogenesis and vasculogenic mimicry of pancreatic ductal adenocarcinoma via disrupting the YAP-TEAD complex. *Cancer Sci* 2017; **108**:478–487.

Downloaded from http://journals.lww.com/anti-cancerdrugs by BhDMf5ePHKav1zEoum1tQfN4a+kJLhEZgbsIHo4XMi0hCywCX1AWnYQp/IlQrHD3i3D0OdRyi7TvSFl4Cf3VC4/OAVpDDa8K2+Ya6H515kE= on 07/02/2024